AIAA SciTech Forum
6-10 January 2020, Orlando, FL
AIAA Scitech 2020 Forum

10.2514/6.2020-0467

On the Restricted 3-Body Problem for the Saturn-Enceladus system: mission geometry and orbit design for plume sampling missions

Lotfi Massarweh[1]
Instituto Superior Técnico, Lisbon, 1049-001, Portugal
Deimos Engenharia S.A., Lisbon, 1998-023, Portugal

Paolo Cappuccio[2]
University of Rome Sapienza, Rome, 00185, Italy

Enceladus has been identified as one of the most interesting targets for future space missions after plume ejecta were discovered in the Tiger Stripes region. Many concepts, aiming to search for habitable zones beyond Earth, require passing through this plume to collect samples of the ejecta. This orbit design is not a trivial task due to the vicinity of Enceladus to Saturn, which causes non-negligible third body perturbations and strongly deflects the orbit of a spacecraft around Enceladus. In this paper we address this problem by extensively studying the Circular Restricted Three Body Problem and linearly stable Halo orbits passing close over Enceladus' South Pole. Some resonance solutions are then evaluated considering the elliptical problem and, finally, a preliminary validation is given by integrating the spacecraft in a model based on latest planetary/satellite ephemerides.

I. Introduction

Discovered in 1789 by the astronomer Frederick William Herschel [1], Enceladus is the sixth-largest and second-nearest moon of Saturn. Named after the Greek mythological giant Enkélados, it is one of the most reflective bodies of the Solar System, as a result of the fresh and clear ice dominating its surface. In fact, due to its reflectivity, this icy moon has an estimated surface temperature of around –200° Celsius. [2]

A. Historical context

The first close-up images of Enceladus were made by the U.S. Voyager program [3], with the intent of studying the outer Solar System, based on two space probes: Voyager 1 and Voyager 2. An initial characterization of Enceladus' surface started in November 1980 with Voyager 1 performing a fly-by maneuver at a distance of around 202040 km [4]. Almost one year after, in August 1981, the spacecraft Voyager 2 passed much closer, at around 87010 km [5], therefore it acquired higher resolutions images of its 'young' surface. Indeed, those images presented a surface with different regions, as also heavily cratered at mid/high-norther latitude regions.

It was only in February 2005 that the Cassini–Huygens space research mission [6] made its first close encounter with Saturn's moon, as collaboration between National Aeronautics and Space Administration (NASA), European Space Agency (ESA) and Italian Space Agency (ASI). NASA's Cassini probe unveiled many mysteries, and soon it revealed that Enceladus is an active moon that hides a global ocean of liquid salty water beneath its crust [7]. The magnetometer aboard the spacecraft showed a strange anomaly [8], similar to an atmospheric plume originating from the moon, pushing against Saturn's magnetic field. The latter motived multiple fly-by maneuvers between 2005 and 2015, thus yielding to significant discoveries, e.g. traces of hydrocarbons venting from the geologically active South Polar Region [9].

[1] Corresponding Author, Marie-Curie Ph.D. candidate at Deimos Engenharia in Lisbon (Portugal), AIAA Student.
[2] PhD student, Mechanical and Aerospace Department, AIAA student.

The south polar terrains revealed, as described in Ref. [10], a landscape "littered with house-sized ice boulders, carved by tectonic features unique to Enceladus and almost entirely free of impact crates". So-called *tiger stripes* were identified as four sub-parallel, linear depressions flanked on each side by low ridges. The Composite Infrared Spectrometer (CIRS [11]) on-board instrument detected thermal emission in these areas, providing means to detect possible endogenic activities, almost 25 years after the thermal radiation measurements provided by Voyager 2. In addition to that, with its third fly-by, completed on the 14th of July 2005 [2], the atmospheric plume at a distance of around 170 km was (for the first time) analyzed by Cassini's Ion and Neutral Mass Spectrometer (INMS [12]). More than a decade later, in October 2015, with a much deeper fly-by maneuver (below 50 km) Cassini was capable of re-analyzing the plume's composition and identifying unambiguously both hydrogen and methane contents as evidence of the (possible) habitability of the internal sea. [13]

These discoveries have triggered several investigations on designing novel mission concepts in order to perform similar fly-by operations and/or with the objective of analyzing in-situ composition of the ejected plume. Indeed, many new concepts have been proposed since 2006, while in particular two proposals have been presented for the NASA New Frontiers program 5 [14], within the theme "Ocean Worlds". The first one is the Enceladus Life Finder (ELF [15]), as an astrobiology orbiter to Enceladus, and the second one is the Enceladus Life Signatures and Habitability (ELSAH [16]). Unfortunately, both were not selected, whereas the Dragonfly concept [17] was assigned as New Frontiers Mission planned for 2034. Supposedly, the latter will send a mobile rotorcraft on the surface of Titan, the largest moon of Saturn, with the objective of understanding its organic and methanogenic cycle, as it relates to prebiotic chemistry [18]. More and more new concepts are being continuously proposed, especially targeting Europa, Jupiter's moon, and indeed Enceladus.

According to the Planetary Science Decadal Survey (2013-2022) defined in 2011 [19], the unanswered question is if "beyond Earth, are there contemporary habitats elsewhere in the solar system with necessary conditions, organic matter, water, energy, and nutrients to sustain life, and do organisms live there now?". Recent discoveries regarding the ingredients of amino acids within the plumes compound at Enceladus have been made (see Ref. [20]), and a fifth New Frontiers Announcement of Opportunity is expected to be released in few years from now.

B. Research problem heritage

Nowadays, one of the main challenges for a potential exploration of Saturn's system is given by the complicated orbital dynamics modeling needed to reduce substantially overall mission's costs. In this context, costs refer to propulsive maneuvers for trajectory corrections or, more simply, to delta-v budget required for different mission's operations. In particular, the long journey from Earth to Saturn Orbit Insertion (SOI) has been long investigated for more than 40 years now, whereas a first fly-by [21] was performed by NASA's Pioneer 11 robotic space probe already back in September 1979. The power availability is certainly one of the major limitations for the exploration of outer planets (and their satellites), while more recently a re-discussion took place over the possible adoption of fission power in future space missions in support to deep space navigation and exploration. [22]

In general, optimization of delta-v budget could lead to a longer time-of-flight, which has been briefly examined in Ref. [23], thus presenting several design options defined with an arrival date spanning between 2032 and 2040. Moreover, similar aspects were already investigated [24,25] by the Jet Propulsion Laboratory (JPL) at the beginning of 2010 in support to the SS2012 Planetary Science Decadal Survey. In Ref. [24], three key operational phases were identified with a preliminary estimation of 8.5 years to reach the SOI, exploiting Venus fly-by maneuvers, and an additional 3.5 years to reach the Enceladus Orbit Insertion (EOI) again making use of Saturn's moons' close fly-bys.

In the current research work we will not consider aspects such as the transfer from Earth to SOI, and/or from SOI to EOI. However, it should be underlined that those are critical aspects of any space mission design, while few alternative designs of trajectory for EOI were also extensively studied in Ref. [26], making use of the gravity-assists of low-mass Saturnian moons Rhea, Dione and Tethys. Indeed, the investigation proposed here focuses on possible trajectories to enable science-based operations and further investigation of plume ejecta in the tiger stripes region near Enceladus' South Pole. These trajectories are so defined based on linear stability criteria and few additional key parameters relevant for an ideal space sample-retrieval mission by means of a low-altitude flying orbiter.

The orbital stability around a planetary satellite has been studied for long time, as both analytical and numerical approaches have been usually employed (see Ref. [27]). Some complications arise from the moment that analytical solutions are not easily accessible when considering the dynamical motion under the influence of a third body. In particular, for systems with the orbiting (planetary) satellite mass substantially smaller than the main planet's mass (e.g. Enceladus *versus* Saturn or Europa *versus* Jupiter), a possible option is to consider the Hill problem as limit version of the well-known Restricted 3 Body Problem (R3BP [28]). Even so, the model adopted suffers of many non-negligible effects, such as the non-spherical gravity perturbations caused by both primary (here Saturn) and secondary (here Enceladus) masses and/or relativistic corrections.

A first complete assessment of possible science orbits was performed by Russel and Lara (see Ref. [29]), based on a Hill model where J2-effects were taken into account, along with other higher-order terms. In that work, the orbits, previously generalized to several planetary satellite systems by Sheeres et al. [27], were extensively discussed and investigated for the Saturn-Enceladus system. In this way, the definition of resonance (periodic, stable) solutions was possible in view of near-polar excursions for plume experiments. High-inclination trajectories were identified within a Hill problem, later numerically continued in order to consider Enceladus oblateness effects. In addition to that, their stability was assessed over a six months period involving also Saturn J2-effects as well as for main gravity accelerations from Sun, Jupiter and Titan, the largest moon in the Saturnian system.

The aforementioned (stable) solutions were later extended in Ref. [30], aiming to very-low-altitude and very-high-inclination trajectories in order to enable geodesy science at Enceladus. Nonetheless, no oblateness effects were considered, (poorly) justified by the uncertain nature of the J2-parameters for this Saturn's icy moon. In that research work, most of the trajectories orbiting around the secondary mass (here Enceladus) were considered at an altitude of 21km, whereas no other solutions, e.g. Halo family of trajectories, were deeply analyzed.

The applicability of Halo solutions, as suggested in Ref. [29] is therefore investigated here, along with other well-known continuous families of periodic solutions existing in the Circular R3BP (CR3BP). Their linear stability is an important indicator of the local behavior, especially due to the so-called *unstable* manifolds [31] that represent an obstacle, if not properly considered, to station-keeping maneuvers in low-cost missions. The extension of those continuous families into the Elliptical R3BP (ER3BP) is possible only when resonance conditions are maintained [32], while the bifurcation of periodic solutions in the ER3BP is also discussed. In this model, the eccentricity of the secondary mass can be taken into account for a better design of future science orbits. Validation and discussion of these periodic (resonance) solutions is based on few preliminary simulations performed by making use of a more accurate dynamical model [33].

C. Paper structure

In Sect. II, the principal methodologies are presented, and the mathematical background for both the Circular and the Elliptical R3BP is given. A brief discussion on existing periodic solutions takes place here; moreover some periodicity conditions are briefly delineated. In Sect. III, the process of generation of periodic orbits is introduced for both R3BPs. In Sect. IV, the main results relative to the CR3BP for the Saturn-Enceladus system are presented and discussed. Main insights on the linear stability of those solutions are given making use of Dynamical System Theory (DST), while additional operational constrains on these closed trajectories are also introduced. In Sect. V, the analysis of the ER3BP is given together with a validation making use of a more realistic simulation setup, e.g. considering an ephemeris model. Last, within Sect. VI, the principal conclusions of this research work are given along with recommendations for future work.

II. Methodology

Most of the methodologies here presented are taken from Ref. [34]. When considering dynamical systems with three bodies, e.g. a planet, its satellite and an orbiting spacecraft, the latter usually has a negligible impact on the orbital motion of the two celestial bodies. In this case we refer to a *restricted* three-body problem [28], therefore both two masses, still described here as point-like, will orbit around the system's barycenter following trajectories defined by a Kepler-like model [35]. Without external forces, their motion is so defined by specific curves bounded within a planar plane, which mostly depends upon the initial conditions. However, it should be clear that the solution here refers to the barycenter of the entire system. At the same time, a very similar solution to this 2-Body Problem (2BP) can be expressed in terms of relative distance, therefore being modeled as a so-called Kepler problem.

In the R3BP, even if the perturbation due to the secondary mass on the primary one is small, it still shall be taken into account [35]. When considering a bounded motion, i.e. elliptic trajectories, we can define an invariant plane and an orthogonal direction, the latter aligned with the angular momentum vector of the system. As a consequence, a rotating system can be so constructed (see Figure 1), where the x-axis is aligned with the direction from the primary to the secondary mass, the z-axis is orthogonal to this fixed plane and the y-axis completes the right-hand system. As stated, the origin of this synodic system corresponds to the barycenter.

At this point two cases should be discussed. In fact, the orbital motion defined by Saturn and Enceladus around their mutual barycenter could be modeled as an Ellipse or a Circle, leading to the ER3BP or CR3BP, respectively. Even if the Elliptical case is more accurate, in general is also much more complicated due to an explicit time-dependency in the differential equations of the spacecraft (S/C) motion. We define the S/C dynamics in the synodic system, where Saturn is given as $\boldsymbol{P_1} = [x_1, 0, 0]$, Enceladus as $\boldsymbol{P_2} = [x_2, 0, 0]$ and the S/C as $\boldsymbol{P_3} = [x, y, z]$.

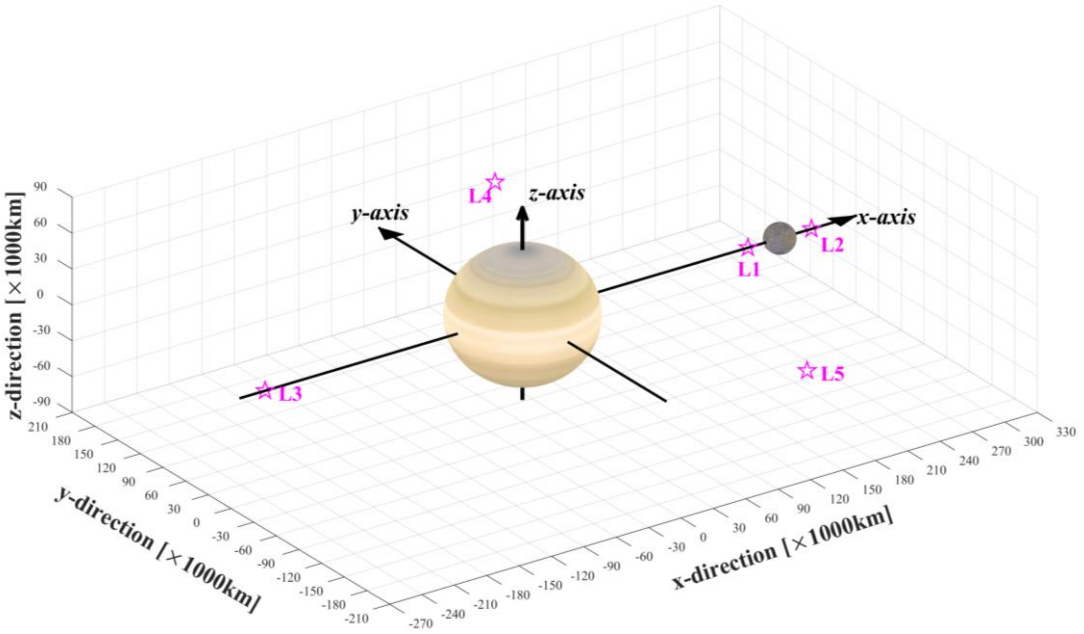

Figure 1: The synodic barycentric reference frame used for the Circular and Elliptical R3BP. In magenta the Lagrange points of the CR3BP have been illustrated. For graphical purposes, dimensions of Enceladus (and L1/L2 distances) are enlarged by a factor 50. Note that the rotation around the z-axis is counterclockwise.

It can be shown, following Ref. [34], that three second-order non-linear Ordinary Differential Equations (ODEs) are retrieved. Those equations, considering all derivatives with respect to time $t \in \mathbb{R}$, are given as

$$\frac{d^2}{dt^2}\begin{pmatrix} x \\ y \\ z \end{pmatrix} \equiv \begin{pmatrix} \ddot{x} \\ \ddot{y} \\ \ddot{z} \end{pmatrix} = -\mu_1 \cdot \frac{\boldsymbol{r_{13}}}{r_{13}^3} - \mu_2 \cdot \frac{\boldsymbol{r_{23}}}{r_{23}^3} - \begin{pmatrix} -2\omega \cdot \dot{y} \\ +2\omega \cdot \dot{x} \\ 0 \end{pmatrix} + \begin{pmatrix} \omega^2 \cdot x \\ \omega^2 \cdot y \\ 0 \end{pmatrix} - \begin{pmatrix} -\alpha \cdot y \\ +\alpha \cdot x \\ 0 \end{pmatrix} \tag{1}$$

with $\mu_1, \mu_2 \in \mathbb{R}$ as standard gravitational parameters for Saturn and Enceladus, respectively. Moreover, we have the angular velocity of the system given as $\omega = \omega(t) \in \mathbb{R}$, which is time-varying for the elliptical case. It follows here the definition of an angular acceleration, expressed as $\alpha = \alpha(t) \in \mathbb{R}$. The distances $\boldsymbol{r_{13}}, \boldsymbol{r_{23}}$ refer to vectors going from the masses' position vectors $\boldsymbol{P_1}, \boldsymbol{P_2}$ to the spacecraft position vector $\boldsymbol{P_3}$ at a certain instant.

The reader should be aware that the expressions for ω and α are well-defined, as computed from the Kepler motion of the two masses. These two equations are given in Ref. [35], and after few manipulations we can write

$$\omega = \frac{d\theta}{dt} = n \cdot \frac{(1 + e \cdot \cos\theta)^2}{(1 - e^2)^{3/2}} \tag{2}$$

$$\alpha = \frac{d\omega}{dt} = \psi \cdot \omega^2, \qquad \forall \psi = -\frac{2e \cdot \sin\theta}{1 + e \cdot \cos\theta} \tag{3}$$

with $\theta \in \mathbb{R}$ as true anomaly, increasing counterclockwise, while other orbital parameters are $e \in \mathbb{R}$ as eccentricity and $n \in \mathbb{R}$ as mean angular motion of the rotating system. As known, for the circular case we have that $\omega = n$, meanwhile $\alpha = 0$ since the synodic system rotates uniformly around the z-axis. The mean motion of the system can be also expressed by Kepler's Third Law [36], so inversely proportional to the orbital period $T \in \mathbb{R}$, such that

$$n = \frac{2\pi}{T} \equiv \sqrt{\frac{\mu_1 + \mu_2}{a_{12}}} \tag{4}$$

where $a_{12} \in \mathbb{R}$ is the semi-major axis of the Keplerian orbit of the secondary mass (Enceladus) around the primary one (Saturn). At this point we can firstly present the dynamical model for the CR3BP, in order to later extend it to the elliptical case (ER3BP), without any constrains on the aforementioned Kepler parameters.

A. Circular Restricted 3 Body Problem (CR3BP)

A simple manipulation allows writing the previous ODEs in a non-dimensional form, where we define a spatial unit as a_{12}, a temporal unit as n^{-1} and, last, a mass unit as $M_{tot} = M_1 + M_2$. It follows (in Ref. [34]) that the orbital period is now expressed as $T = 2\pi$, and $\mu_1 + \mu_2 = 1$. Moreover, considering the notation $\mu = \mu_2$, we can also write $\mu_1 = 1 - \mu$, while the last term (related to the angular acceleration) cancels out in Eq. (1). It follows that

$$\begin{cases} \ddot{x} = x - (1-\mu) \cdot \dfrac{(x+\mu)}{r_1^3} - \mu \cdot \dfrac{(x+\mu-1)}{r_2^3} + 2\dot{y} \\ \ddot{y} = y \cdot \left[1 - \dfrac{1-\mu}{r_1^3} - \dfrac{\mu}{r_2^3}\right] - 2\dot{x} \\ \ddot{z} = -z \cdot \left[\dfrac{1-\mu}{r_1^3} - \dfrac{\mu}{r_2^3}\right] \end{cases} \tag{5}$$

The previous set of differential equations is *autonomous* [37], meaning that it does not have an explicit dependency upon a time-like parameter. In addition to that, it can be shown that within such non-dimensional form, the time-like parameter is actually the true anomaly θ, since it holds that $\theta = n \cdot t$, given $t_0 = 0$. As also visible in Eq. (5), for some specific initial conditions the motion is defined (see Ref. [38]) by three groups of solutions:

1) **Equilibrium solutions**, i.e. critical points of the ODEs;
2) **Periodic solutions**, usually characterized by a specific periodicity interval (or period);
3) **Integral manifolds**, as a set of defined trajectories within the phase-space of the dynamical system.

These results have been well-known for several decades, while extensive and more comprehensive analyses can be found in Ref. [28]. The existence of five equilibrium points, all lying within the invariant plane, is due to Euler and Lagrange (see Ref. [39]) for the so-called collinear and equilateral points, respectively. The three collinear points[3], as shown in Figure 1, lie over the x-axis and are known for their linear instability. The latter means that the initial small perturbation to an equilibrium solution will most likely leads to trajectories following the invariant manifolds of such dynamical system. This could be taken as an advantage in some cases, since these trajectories can be exploited for a low-cost transfer within the same system or even between different ones. [40]

A very important result of past researches is given in Ref. [41], with two theorems linked to symmetries found in these equations of motion. The first theorem, called the "Irreversibility Theorem", states that *if a trajectory is physically possible in the xyz-space, then the reverse trajectory is not physically possible*. This was already observed in Ref. [42], since the Lagrangian is not invariant to this type of "transformation", therefore reverse trajectories are not admitted in the CR3BP. A second theorem, named the "Theorem of Image Trajectory", defines three additional symmetric trajectories, given a first one physically possible. Two trajectories, symmetric with respect to the x-axis and the xz-plane, flow in the opposite sense of the original one. The last one, with respect to the xy-plane, can be observed in Eq. (5) by performing the simple change of variables $z^* = -z$, without varying its expression.

When looking at the periodic motion, especially in a neighborhood of collinear equilibrium points, it follows that for closed trajectories crossing the xz-plane to be periodic, they should have at least two orthogonal passes such that their symmetric reverse orbit exists [44]. This is an important aspect exploited in the selection of initial conditions for the generation of periodic solutions, and it does not depend upon the system selected but holds valid for any CR3BPs. The symmetry with respect to the xy-plane is also fundamental, and very relevant for the existence of a southern and a northern Halo family of periodic solutions at the collinear L-points.

B. Periodic motion near the L-points in the CR3BP

The aforementioned proprieties of the CR3BP allow having insights on the different behaviors of trajectories in the phase-space of the system. Moreover, the use of dynamical system theory has made possible in the past decades to analyze periodic solutions more accurately. This type of trajectories is clearly more suitable for space mission operations given its repetitive pattern, while potentially reducing station-keeping costs for keeping the spacecraft within its nominal (or operative) mission trajectory.

When looking at the collinear L-points, it is know that their local dynamics in the six-dimensional phase-space is not linearly stable. Nonetheless, under the assumption of a linearized motion, two different mono-parametric Lyapunov families of solution can be defined. These ones are *theoretically* bounded within an in-plane and an out-of-plane distinctive motion, while always characterized by a different pulsation, for any μ-value selected. [45]

[3] As mentioned in the text, the collinear points were firstly discover by L. Euler in 1767 with *"De moto rectilineo trium corporum se mutuo attrahentium"*, but usually referred to as Lagrange points, or also L-points. [43]

The reader shall be aware that periodic solutions are not the only ones suitable for a space mission design. In fact, also quasi-periodic trajectories (e.g. Lissajous or Quasi-Halo orbits) have been extensively investigated (see Ref. [46]), and numerically computed in a very efficient way by means of multiple Poincaré sections [47]. In this contribution quasi-periodic solutions have not been considered, mostly due to more complications arising in the assessment of their linear stability. The latter can be investigated by means of an analysis of characteristic multipliers. These are eigenvalues of the State Transition Matrix (STM) propagated along the selected periodic trajectory. In this case we refer more correctly to it as "Monodromy matrix" (or M-matrix), which provides good insights on the behaviors of small initial displacements after a complete revolution of the orbit. [34]

The concept of orbital stability, strongly relevant for the definition of the most suitable orbits, is quite different from the simple definition of Lyapunov stability applied to the periodic motion. The latter concerns the local boundedness of perturbed solutions near the reference periodic one. For the orbital stability however, this condition can also be evaluated with respect to some (local) fixed points, e.g. considering multiple (repetitive) intersections in a Poincaré section. In some literature (see Ref. [38]), the group of intersections is called Poincaré Map, or First Recurrence Map. The displacements from the periodic solution are then evaluated within this (arbitrary) section.

The first approach, based on the M-matrix analysis, has been employed here, considering the following:

1) The CR3BP is a Hamiltonian system, therefore it has a structure denoted as symplectic and it will always present pairs of reciprocal eigenvalues (or characteristic multipliers).
2) The M-matrix has real values, and so the complex eigenvalues $\lambda_i \in \mathbb{C}$ can be found in quadruplets.
3) The M-matrix associated with periodic solutions will always have at least one real $\lambda_1 = +1$, meanwhile an additional $\lambda_2 = +1$ will also exists due to the first (symplectic) property.

The four remaining eigenvalues define the linear stability of each periodic solution, while their respective eigenvectors define indeed particular (admitted) directions of motions. Considering the four complex eigenvalues of the M-matrix, we can end up with three different orders of instability: **0^{th}-order** instability when $|\lambda_i| = 1$ for all the four remaining i-eigenvalues, a **1^{st}-order** or **2^{nd}-order** instability when one pair or two pairs of complex eigenvalues do not lie on the unit circle. Once again, the aforementioned symplectic property assures that if there is a $|\lambda| < 1$, so attracting a nearby trajectory to the periodic solution, there will be also a $|\lambda| > 1$, thus defining a direction of instability. The latter is indeed an unstable manifold that could lead the S/C far away from our preferred solution. It follows that this closed trajectory is less likely suitable as a nominal science orbit, and most probably leads to a high station-keeping cost for corrective maneuvers.

The preferred orbits seem to be the ones presenting 0^{th}-order instability, at least as a first guess. An additional consequence of the Hamiltonian form of the equations (see previous Point 3) is that there is always (at least) one direction involving another periodic trajectory. In short, for each periodic solution there will always be another one in the immediate vicinity and with slightly different initial conditions. This feature of the CR3BP assures continuity in each family of periodic solutions, and in principle this allows having an infinite number of candidate solutions for the exploration of Enceladus. We continue discussing the generation of some families of periodic solutions.

III. Generation of periodic orbits

The examination of the local behavior of collinear Lagrange points (here considering only L1/L2, since closer to the secondary mass) can provide a first-order approximation of the dynamical motion admitted at L-points. Once moving far enough from these equilibrium points, the linearized approach cannot properly describe all admitted trajectories and different techniques shall be employed. The Centre Manifold Reduction, or normal form scheme, has been given in Ref. [48] as a semi-analytic approach to this problem, whereas here we will consider an alternative technique. The method of strained coordinates, also known as Linstedt-Poincaré method [49], is principally focused on periodic solutions in a perturbed differential system defined by a (supposedly small) scalar parameter $\epsilon > 0$.

The LP method was applied in Richardson's paper [50] in order to find a third-order analytic approximation to period motion around collinear Lagrange points. The CR3BP system is so linearized around each L-points and small parameters are defined in terms of amplitude of the (bounded) oscillations around each equilibrium point. As noted, this third expansion made it already possible to approximate the well-known Halo orbital motion, as a bifurcation from the aforementioned in-plane Lyapunov family of solutions. [34]

We refer the reader to Ref. [34] for more details on the algorithm definition for the generation of three families of periodic solution around L1/L2 points of the Saturn-Enceladus CR3BP. Three families are considered, being

1) The Horizontal Lyapunov (H-Lyap) family, arising from the linear in-plane motion at the L-points;
2) The Vertical Lyapunov (V-Lyap) family, arising from the linear out-of-plane motion at the L-points;
3) The Halo family, which consists of both a Northern (N-Halo) and a Southern (S-Halo) group due to the third symmetry previously introduced.

Given a certain μ-value, and after selecting one of the three families, the third-order analytical approximation is computed for a certain L-point. In this way two initial conditions are found, relative to two periodic solutions near the selected Lagrange point. Those guesses are corrected with a Differential Correction (DC) algorithm, originally adopted in Ref. [51] for the generation of Halo trajectories in the Earth-Moon CR3BP. The DC-algorithm is seen as a single shooting method, generalized and well-described in Ref. [45], thus making use of the STM to correct the initial conditions. The latter, as graphically represented in Figure 2, concern two position's components within the xz-plane and an orthogonal shooting velocity. Each initial condition, or IC, is defined as $\boldsymbol{X_0} = \{x_0, 0, z_0, 0, v_{y0}, 0\}$.

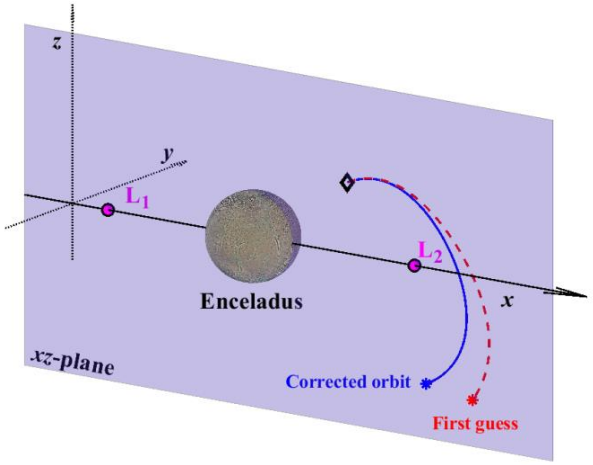

Figure 2: The graphical representation of single shooting method applied to correct initial conditions that are associated to a closed trajectory. As described in the text, this "shooting condition" generally lies within the xz-plane, with an orthogonal velocity vector in one of the two intersections with this symmetry plane.

The use of two solutions $\boldsymbol{X_0^I}$ and $\boldsymbol{X_0^{II}}$ allows defining a third guess by numerical continuation, which can follow two different strategies: a natural parameter or a pseudo-arclength approach. The former will add a step-size to one of the shooting components (e.g. preferably as Δx_0) and use this initial guess within a DC-algorithm, while the other method (here adopted) updates all components for the third guess as follows

$$\boldsymbol{X_0^{III}} = \boldsymbol{X_0^{II}} + \boldsymbol{\Delta X_0}, \qquad \forall \boldsymbol{\Delta X_0} = \boldsymbol{X_0^{II}} - \boldsymbol{X_0^{I}} \tag{6}$$

In this way, the guess is more accurate and the DC-algorithm converges in a smaller number of iterations [52], whereas general polynomial extrapolations (using more ICs) can be used, as given in Ref. [53]. A few conditions are checked in order to assure the periodicity, where assuming a period $T \in \mathbb{R}$ we can define a threshold for the displacement after one revolution (ideally zero for a perfectly periodic trajectory). This threshold is set for both position (ΔP_{max}) and velocity (ΔV_{max}) displacements at $t = T$ for an initial time $t_0 = 0$, such that

$$\sqrt{[x(T) - x_0]^2 + [z(T) - z_0]^2} \leq \Delta P_{max}\,, \qquad \left|v_y(T) - v_{y0}\right| \leq \Delta V_{max}, \tag{7}$$

The target orbital period is not fixed, while later updated with the DC-algorithm. In addition to such "closing conditions", the so-called "eigenvalues condition" is also considered, following Ref. [34].

The analysis of linear stability by checking the eigenvalues of the Monodromy matrix enables a further validation of this periodicity. In fact, for any periodic trajectory, two eigenvalues are constrained to be real and equal to +1. It follows that, if no eigenvalues are found with this value (discarding small numerical errors), then the solution is not considered periodic and the algorithm stops the generation of new members within the family. At the end of the iterative process, a discrete sample of members from each continuous family of periodic solutions is obtained and the linear stability, orbital period, energy level and geometric characteristic can be evaluated.

As mentioned, the symplectic nature of the CR3BP puts constrains on the existence of periodic solutions, mostly found in continuous families. In each family, the local behavior (here intended as linear stability) can be different when considering different members, while the change in order of stability is different once considering alternative μ-values. In Ref. [53] different values are considered, as several families considered also show a bifurcation in the μ-parameter. This was a known result also for the equilateral L-points, where the linearly stable nature of L4/L5 is limited to μ-values smaller than the so-called Routh critical value [54], approximately equal to $\mu_R = 0.03852$.

However, for practical applications it should be noted that variations of the μ-parameters (given as a fraction of the secondary mass over the system's total mass) are usually negligible. For example, when taking into account Enceladus venting activity, from a theoretical point of view it should be considered that the mass of the system is changing in time, as also its μ-value. This variation is extremely insignificant, while also possible uncertainties (whether small) in the μ-value will not sufficiently affect the design of suitable orbital solutions. This aspect is most likely relevant for binary systems, e.g. considering S/C rendezvous close to a contact binary asteroid system [55].

For what concerns the Saturn-Enceladus R3BP system, there are many model deviations from an ideal CR3BP scenario. Indeed, as also mentioned in Ref. [29], the oblateness effects of both Saturn and Enceladus can play a substantial role in the orbital motion of a spacecraft. In addition to that, Enceladus has a non-negligible eccentricity in its Kepler motion around Saturn, in general given approximately[4] as 0.0047.

A. Resonance solutions in the ER3BP

The definition of the Elliptical R3BP is conceptually very similar to what seen from Eq. (1), thus considering a non-zero angular acceleration of the system. Here we follow the formulation given in Ref. [34], with the definition of a time-rescaling with respect to the θ-parameter (as for the CR3BP) and a "pulsating" reference frame. The former simply considers time-derivatives with respect to $\theta \in \mathbb{R}$ as the new time-like parameter of this differential system. The time-rescaling of derivatives for a certain state-vector $\boldsymbol{Q} \in \mathbb{R}^6$ is based on the chain's rule such that

$$\frac{d\boldsymbol{Q}}{dt} = \frac{d\boldsymbol{Q}}{d\theta} \cdot \frac{d\theta}{dt} \equiv \frac{d\boldsymbol{Q}}{d\theta} \cdot \omega, \qquad \forall \omega = \omega(\theta) \tag{8}$$

$$\frac{d^2\boldsymbol{Q}}{dt^2} = \frac{d}{dt}\left[\frac{d\boldsymbol{Q}}{d\theta} \cdot \omega\right] = \frac{d}{d\theta}\left[\frac{d\boldsymbol{Q}}{d\theta} \cdot \omega\right] \cdot \omega \equiv \frac{d^2\boldsymbol{Q}}{d\theta^2} \cdot \omega^2 + \frac{d\boldsymbol{Q}}{d\theta} \cdot \frac{d\omega}{d\theta} \cdot \omega \tag{9}$$

leading in a more compact notation to

$$\dot{\boldsymbol{Q}} = \boldsymbol{Q}' \cdot \omega(\theta), \qquad \ddot{\boldsymbol{Q}} = [\boldsymbol{Q}'' + \boldsymbol{Q}' \cdot \psi] \cdot \omega^2(\theta) \tag{10}$$

with the prime-notation for derivatives with respect to the θ-parameters, the dot-notation otherwise. Moreover, the ψ parameter was already defined in Eq. (3), and it plays a role in the definition of Lagrange points. The definition of a pulsating frame was already suggested in Ref. [28], and has several advantages since Lagrange points can be easily defined (actually numerically the same as the CR3BP) and new symmetry constrains arise in the ER3BP.

The pulsating frame is such that the spatial unit is now the instantaneous distance $r_{12} = r_{12}(\theta)$ between the primary and the secondary masses. It follows that the new coordinates for the S/C position are the followings

$$\boldsymbol{P}_3^* = \frac{\boldsymbol{P_3}}{r_{12}(\theta)}, \qquad \forall r_{12}(\theta) = a_{12} \cdot \frac{(1 - e_{12}^2)}{1 + e_{12} \cdot \cos\theta} \tag{11}$$

with the original vector $\boldsymbol{P_3} = [x_3, y_3, z_3]$ now defined (in the pulsating system) as $\boldsymbol{P_3^*} = [x_3^*, y_3^*, z_3^*]$. Also the S/C velocity in this frame will be expressed differently, where making use of both Eq. (8) and Eq. (11) we can write

$$\frac{d\boldsymbol{P}_3^*}{d\theta} = \frac{d}{d\theta}\left[\frac{\boldsymbol{P_3}}{r_{12}(\theta)}\right] = \ \ldots = \frac{\boldsymbol{P_3'}}{r_{12}(\theta)} + \boldsymbol{P}_3^* \cdot \frac{\psi}{2} \tag{12}$$

We leave to the reader the proof of these relations, as also available in Ref. [34], while here we only provide the expression for retrieving the shooting velocity starting with the ICs computed in the ER3BP, such as

$$\frac{d\boldsymbol{P_3}}{dt} \equiv \dot{\boldsymbol{P}}_{\boldsymbol{3}} = r_{12}(\theta) \cdot \omega(\theta) \cdot \left[\frac{d\boldsymbol{P_3^*}}{d\theta} - \boldsymbol{P}_3^* \cdot \frac{\psi}{2}\right] \tag{13}$$

and it should be noted that the auxiliary variable ψ is zero for θ values such that $\sin\theta = 0$. As verification, for the CR3BP case the transformation is always found (still considering a dimensional form) as follows

$$\dot{\boldsymbol{P}}_{\boldsymbol{3}} = a_{12} \cdot n \cdot \frac{d\boldsymbol{P_3^*}}{d\theta} \equiv a_{12} \cdot n \cdot \frac{d}{d\theta}\left[\frac{\boldsymbol{P_3}}{a_{12}}\right] = n \cdot \boldsymbol{P_3'} \tag{14}$$

[4] The approximate planetary data is available at "Enceladus: Facts & Figures". Solar System Exploration, National Aeronautics and Space Administration, August 12th, 2013. Retrieved online on December 1st, 2019.

The final expression of the pulsating (time re-scaled) differential system for the ER3BP is summarized such as

$$\begin{cases} \dfrac{d^2x^*}{d\theta^2} = +\dfrac{1}{1+e_{12}\cdot\cos\theta}\left[x^* - (1-\mu)\cdot\dfrac{(x^*+\mu)}{r^{*3}_1} - \mu\cdot\dfrac{(x^*+\mu-1)}{r^{*3}_2}\right] + 2\cdot\dfrac{dy^*}{d\theta} \\ \dfrac{d^2y^*}{d\theta^2} = +\dfrac{y^*}{1+e_{12}\cdot\cos\theta}\cdot\left[1 - \dfrac{1-\mu}{r^{*3}_1} - \dfrac{\mu}{r^{*3}_2}\right] - 2\dfrac{dx^*}{d\theta} \\ \dfrac{d^2z^*}{d\theta^2} = -\dfrac{z^*}{1+e_{12}\cdot\cos\theta}\cdot\left[\dfrac{1-\mu}{r^{*3}_1} - \dfrac{\mu}{r^{*3}_2} + e_{12}\cdot\cos\theta\right] \end{cases} \quad , \quad \forall {r^*}_i = \frac{r_i}{r_{12}(\theta)} \tag{15}$$

where the existence of equilibrium points within the ER3BP (for this formulation) is visible since the expression in the parenthesis on the right side is algebraically equivalent to the one given in Eq. (5) for the CR3BP. It is also clear that this formulation holds only for (positive) eccentricity values below 1, while in the limit case for $e_{12} = 0$ we get back the same dynamical system of the CR3BP. To observe that this is a *non-autonomous* differential system since it explicitly depends upon the main time-like parameter, here being the θ-variable.

The existence of a periodic solution for this system requires that the shooting condition is fixed at a time

$$\theta_0 = k\cdot\pi, \qquad \forall k \in \mathbb{Z}\ (\text{integer}) \tag{16}$$

with 2π still being the orbital period of Enceladus around Saturn considering an elliptical trajectory. Such a new requirement on the symmetry of trajectories leads to an "Elliptic Periodicity Criterion", formulated in Ref. [56] as an extension of the "Strong Periodicity Criterion", firstly formulated for the planar-ER3BP in Ref. [57]. In general, the condition to have a periodic solution is to have its period in resonance with the motion of the two main masses. With N as number of revolutions for Enceladus, and M as number of revolutions for the S/C, we need that

$$T_C = 2\pi\cdot\frac{N}{M}, \qquad \forall\{N,M\} \in \mathbb{Z}^+\ (\text{positive integers}) \tag{17}$$

where T_C is the period of the closed trajectory in the CR3BP, while the period of the possible resonance trajectory is

$$T_E = M\cdot T_C \overset{\text{def}}{\equiv} 2\pi\cdot N \tag{18}$$

The candidate resonance solutions from the CR3BP are so found within the continuous family, e.g. retrieving with a spline interpolation the ICs of orbits closest to the target resonance one. This gives us approximated shooting conditions that can be processed by a modified DC-algorithm (see Section 4.4.2 in Ref. [34]), which will not consider anymore the period as uncertain but will try to correct the previous vector $\boldsymbol{X_0^{MN}}$ relative to an MN-orbit.

A small remark is given here in support to an efficient orbit design and extension of orbits to the ER3BP, from the moment that numerical problems could arise in the computation of less stable orbits. As mentioned, many periodic solutions can have very unstable manifolds in their neighborhood and due to limited numerical precision the initial conditions could degenerates very quickly after few revolutions. As consequence of this, in general it is convenient to select orbits with zeroth-order (linear) stability, and the divergence behavior of solutions is strongly mitigated as it will be shown in the next section.

The extension of resonance solutions (only periodic trajectories surviving in the ER3BP) makes use again of a numerical continuation scheme. We start with the initial vector $\boldsymbol{X_0^{MN}}$, corrected by the modified DC-algorithm, and we gradually increase the eccentricity value. At each step we follow the same procedure as for the CR3BP, while the first eccentricity is set really small to use the pseudo-length approach for the initialization of new initial conditions in the ER3BP. The eccentricity is also a bifurcation parameter for $e_{12} \to 0$, and two periodic solutions are possible depending upon the initial shooting time, being $\theta_0 = 0$ or $\theta_0 = \pi$. In addition to that, depending on M, for each shooting time we can have two different situations, which have been summarized in Table 1.

Table 1: Four cases are given when extending a resonance solution into the ER3BP, depending on the value of M. Starting in the CR3BP, if M is *even* then the bifurcation depends on which xz-intersection is considered, so having a different shooting sign. If M is *odd* then the bifurcation depends upon the initial shooting time θ_0.

Family Type	M-value	θ_0-value	$r_{12}(\theta_0)$	y-shooting for L1 / L2
Left-group	Even	0	Peri-apsis	Positive / Negative
Right-group	Even	0	Peri-apsis	Negative / Positive
Apo-group	Odd	π	Apo-apsis	Positive / Positive
Peri-group	Odd	0	Peri-apsis	Positive / Positive

IV. Results in the CR3BP model

At this point we can introduce the results for the Saturn-Enceladus system, but firstly the main orbital parameters are provided and briefly discussed. In support to defining a more realistic scenario, both the planetary and the satellite ephemeris are taken from NASA's Navigation and Ancillary Information Facility (NAIF [58]). In particular, the data refers to the latest Saturnian satellite ephemeris from the Saturn Global Fit[5], here named SAT425, which refers to the JPL Development Ephemeris number 438 (DE438). The latter is based on DE430 documented within the JPL Interplanetary Network Progress Report 42-196 [59].

From the satellite ephemeris file (SAT425), the standard gravitational parameters for Enceladus and Saturn are taken, along with main relevant orbital parameters of the system. For the scope of this work, we have retrieved 20 years of data, spanning from 2030 to 2050, which seems reasonable for a future space exploration mission in the Saturnian system. Following literature guidelines, as given in Sect. I (see Ref. [23-24]), we consider here a possible mission arriving at Enceladus Insert Orbit in November 2040. This should be considered simply as a case study for the science orbit design exercise introduced in this research work.

In Figure 3 the relevant orbital parameters are given as variations from the mean values taken over a two weeks period, starting on the 15th of November 2040. During this time span, Enceladus completes more than 10 full revolutions around Saturn, given its orbital period approximately equal to 33 hours. The variations in the semi-major axis (distance between Saturn and Enceladus for the CR3BP) are quite small and limited within few kilometers. As a consequence of this, the orbital period is also quite stable. It is visible, as also well-known in literature [60], that the orbital eccentricity has very large displacements with respect to the 14-days mean value.

An evaluation of the data over the entire 2040 showed also a positive drift for the eccentricity parameter, which is around 271 parts per billion for each Enceladus revolution. In fact, Enceladus is trapped in an orbital resonance with Dione which excites its orbital eccentricity. It is damped by tidal forces, tidally heating its interior and driving the geological activity [61]. In Table 2, the principal parameters for the Saturn-Enceladus system have been summarized

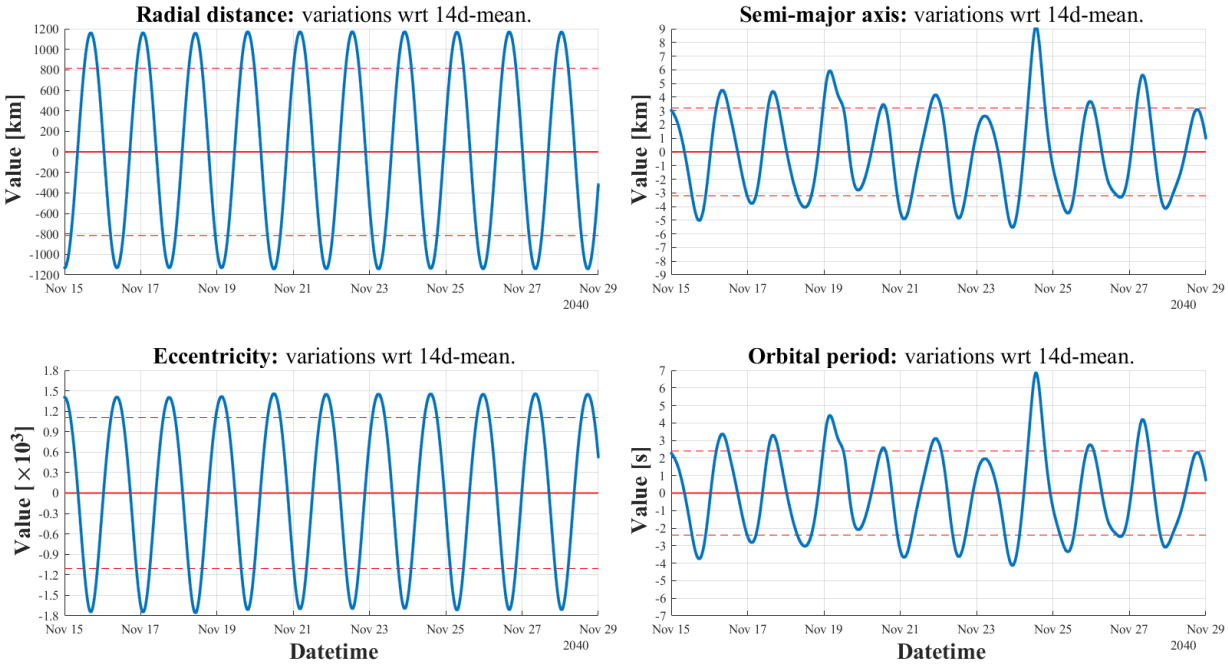

Figure 3: The variations of four orbital quantities are given with respect to their mean value (continuous red line) computed over a two weeks period starting on the 15th of November 2040. The dashed lines in red color represent the standard deviation of these quantities considering the two weeks period. Data has been taken from the SAT425/DE438 ephemeris, while we refer the reader to the text for more details.

[5] The official description is available at https://naif.jpl.nasa.gov/pub/naif/generic_kernels/spk/satellites/sat425.cmt, uploaded on the 28th of August 2019.

Table 2: The main parameters retrieved from the SAT425/DE438 ephemeris file as described in the text. Both the mean value and the standard deviation are given considering two different time spans, both having a sampling time of 1 minute. The values for the 2 weeks period have been used for all the calculations.

Standard gravitational parameter	**Units**	**Reference value used (SAT425/DE438)**	
Enceladus (#602)	km^3s^{-2}	7.210561107781245	
Saturn (#699)	km^3s^{-2}	3.793120627544314e7	
Orbital parameter over 1 year in 2040	**Units**	**Mean value**	**Standard deviation**
Saturn-Enceladus radial distance	m	238038774.031	809456.395
Semi-major axis	m	238411336.318	3154.260
Eccentricity	10^{-3}	4.935884	1.103842
Orbital Period	s	118760.47	2.36
Orbital parameter over 2 weeks from 15/11/2040	**Units**	**Mean value**	**Standard deviation**
Saturn-Enceladus radial distance	m	238021103.842	815646.625
Semi-major axis	m	238411468.296	3206.122
Eccentricity	10^{-3}	4.985714	1.105758
Orbital Period	s	118760.57	2.40

The time-variations of mean elements represent a non-negligible problem, and most likely it will lead to some model's displacements with respect to both CR3BP and ER3BP. A non-dimensional gravitational parameter μ is then computed starting from values in Table 2, so being equal to

$$\mu = 1.90095713928102 \cdot 10^{-7} \tag{19}$$

Without loss of generality, the semi-major axis and eccentricity values considered for the CR3BP and ER3BP are the mean values computed over the two weeks, so having $a_{12} = 238411468.296$ and $e_{12} = 0.004985714$.

A. Periodic solutions for the CR3BP at L1/L2

As visible in Figure 4, three families are generated for each Lagrange points near Enceladus. In the two plots, the Horizontal Lyapunov (in red), the Vertical Lyapunov (in green) and the Northern Halo family are shown. The Northern Halo family is symmetric with respect to the xy-plane, therefore a Southern Halo family could be obtained by changing the sign for the z-variable, as it was described within Sect. II.

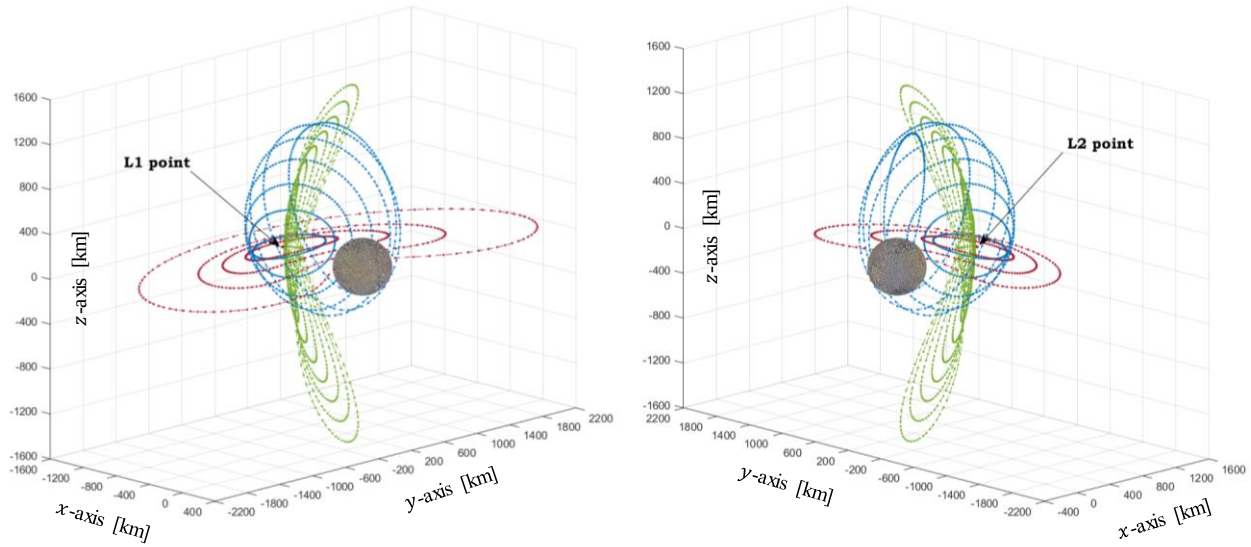

Figure 4: The graphical representations of periodic solutions found in each family near L1/L2 equilibrium points. In red Horizontal Lyapunov, in green Vertical Lyapunov and in blue the Northern Halo family. The initial conditions (lying within the xz-plane) are separated by around 190 km between members in the plots.

The members of each family in Figure 4 have been sampled from a continuous family generated with small position displacements over the xz-plane. As stated, the numerical continuation over a small interval makes sure that the new ICs are close enough to the ideal ones. In this simulation periodic solutions are "shifted" by 4e-7 (in the non-dimensional representation) on the xz-plane, which is equivalent to having member-solutions that are separated by almost 100 meters difference. This result follows the conversion of the length unit, in this case referring to the semi-major axis value of the Saturn-Enceladus system. In Figure 4 a single orbit every 1000 members has been illustrated for graphical clarity, therefore the xz-distance between consecutive ICs in those plots is around 95 km.

What is remarkable is that the entire analysis over the CR3BP does not require the knowledge on the numerical value of semi-major axis, so it holds for systems with a very similar non-dimensional μ-parameter. The linear stability is analyzed looking at the characteristic multipliers of the periodic solutions. As mentioned, those are the eigenvalues of the Monodromy matrix propagated along a certain periodic trajectory, which was previously found with the DC-algorithm.

The symplectic nature of the CR3BP has been already discussed, while it is also visible in the existence of reciprocal values within Figure 5. In each plot a family of solutions is considered, and the absolute value of the characteristic multipliers is shown. It should be noted that two of those eigenvalues are real and equal to +1, while the others are complex-valued. In this work we will not further discuss the orbital properties linked with the complex part and its geometrical meaning, along with bifurcations along each family. The latter has been deeply investigated in Ref. [34] for the Earth-Moon CR3BP and it is not so much relevant for the scope of this research work.

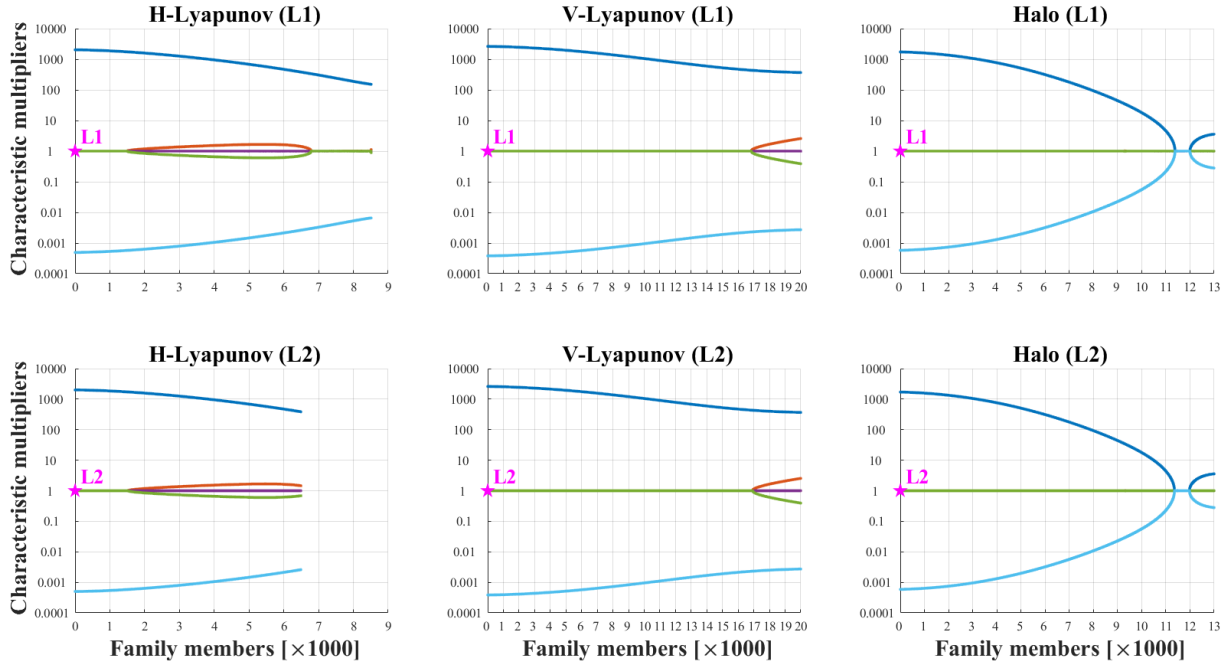

Figure 5: The analysis of linear stability for the six families of periodic solutions has been shown based on the absolute values of their characteristic multipliers. For each value larger than 1, there is always a reciprocal value due to the symplectic nature of the CR3BP. See text for more details on this analysis.

As visible in Figure 5, most of the members in each family present a 1st-order and/or 2nd-order linear stability. In fact only for the Halo case we have a small region with zeroth-order stability. To be more precise, a threshold shall be defined due to the fact that at bifurcations points, where the stability orders change, it is very difficult to well-define whether numerical errors are actually affecting the computation. A condition has been defined here such that when $|\lambda_i| > 1.001$, then the instability order is increased. In Figure 6, the previous plots for the Halo family (for L1 and L2) have been reproduced with a different scale to inspect the small zeroth-order instability region found.

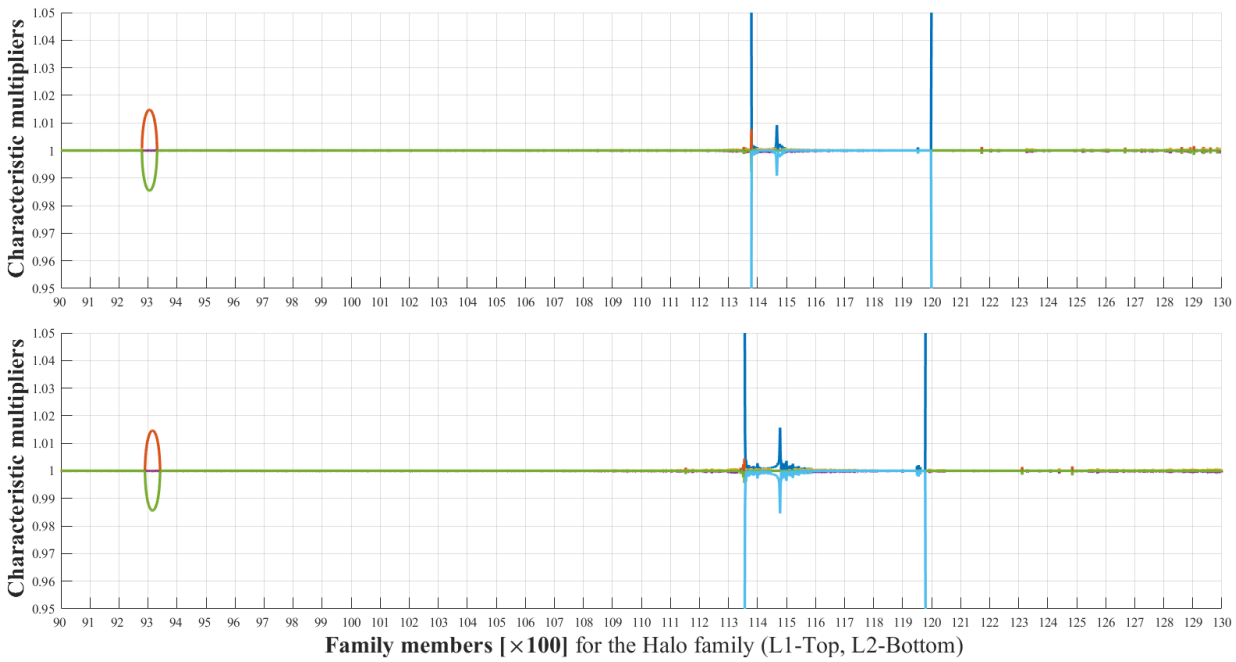

Figure 6: The modules of each characteristic multiplier for the Halo family at L1 (TOP) and L2 (BOTTOM) are shown near the value one. The zeroth-order instability region is discussed in more details within the text.

It is visible that the zeroth-order instability region (Figure 6) has still some characteristic multipliers with module slightly larger than one. Moreover, close to members 9300-9350 we have also a peculiar behavior, with a bifurcation that increases the order of instability. The latter is a Period-Doubling (or Flip) bifurcation where a new periodic solution can arise with a period twice as the original period (see Ref. [34]).

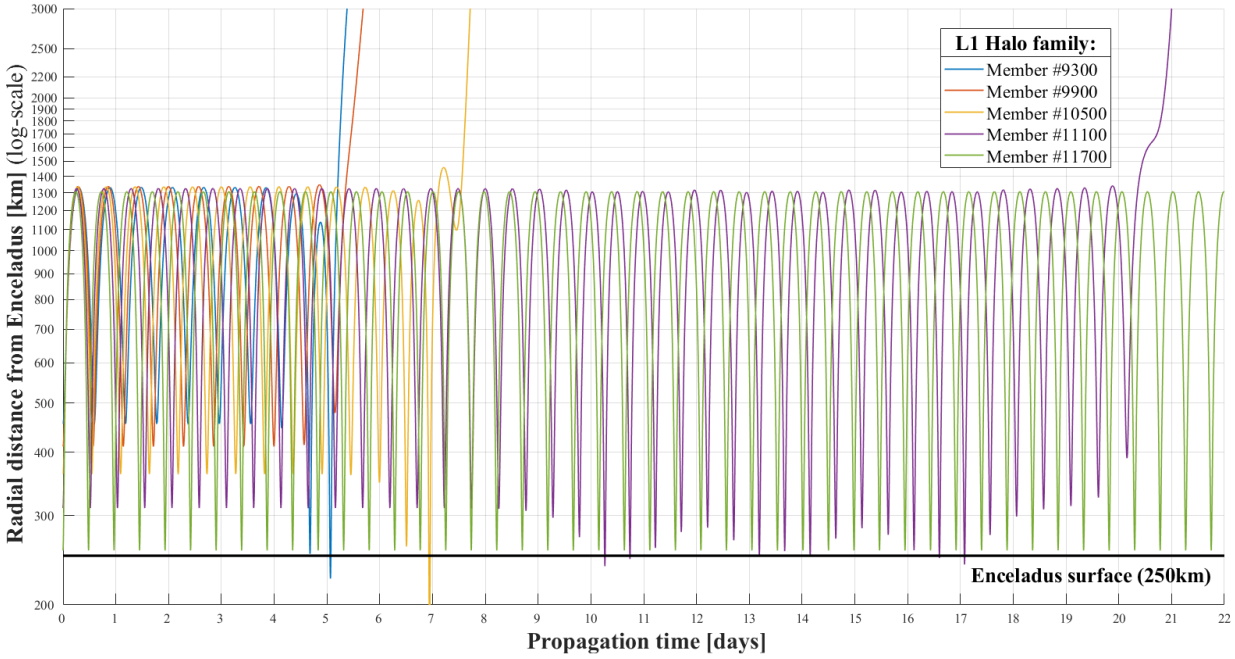

Figure 7: Periodic trajectories of the Halo family at L1 are propagated over 22 days, and their radial distance from Enceladus is shown. It should be observed that the Member #11700 is the only one having zeroth-order instability, therefore its periodic behavior perfectly holds for the entire simulation period.

In this research the zeroth-order instability is further discussed since most likely leading to much more stable orbits that could be exploited for science operations in support to the exploration of the Saturn's icy moon. A last small analysis, presented in Figure 7, shows some members of the Halo family at L1 propagated for 22 days (or 16 Enceladus revolutions) under the CR3BP dynamics. The radial distance from Enceladus is shown and it is visible that the Member #11700, which was the only one with zeroth-order instability, performs better in terms of orbit's repeatability. The other periodic solutions found were either crashing into Enceladus, or diverging in the unstable manifolds mentioned before.

Before discussing the existence of resonance solutions within this (linearly) stable set of solutions, it is important to add some constrains to the mission design problem here discussed. In fact, some of those solutions are actually at a radial distance (from Enceladus' center-of-mass) that is smaller than Enceladus' radius. Another aspect concerns the robustness of this periodic trajectory, where clearly uncertainty in the dynamics parameters could further limit the applicability of missions flying at extremely low altitudes (e.g. hundreds meters over the tiger stripes region).

In Figure 8 the members of the Southern Halo family (at L1/L2) with zeroth-order instability have been shown in green color, while in black color we have members at the edges (i.e. bifurcations) of this set of solutions. It can be observed that solutions are really close to the Enceladus South Polar region, which is of high interest to the scientific community due to cry-volcanic activity at the Tiger Stripes region. Nonetheless, not all solutions are feasible since some of them are actually colliding with Enceladus surface. The continuity of this set of (spectrally) stable solutions allows finding infinite trajectories, at least when considering a dynamics described by the CR3BP.

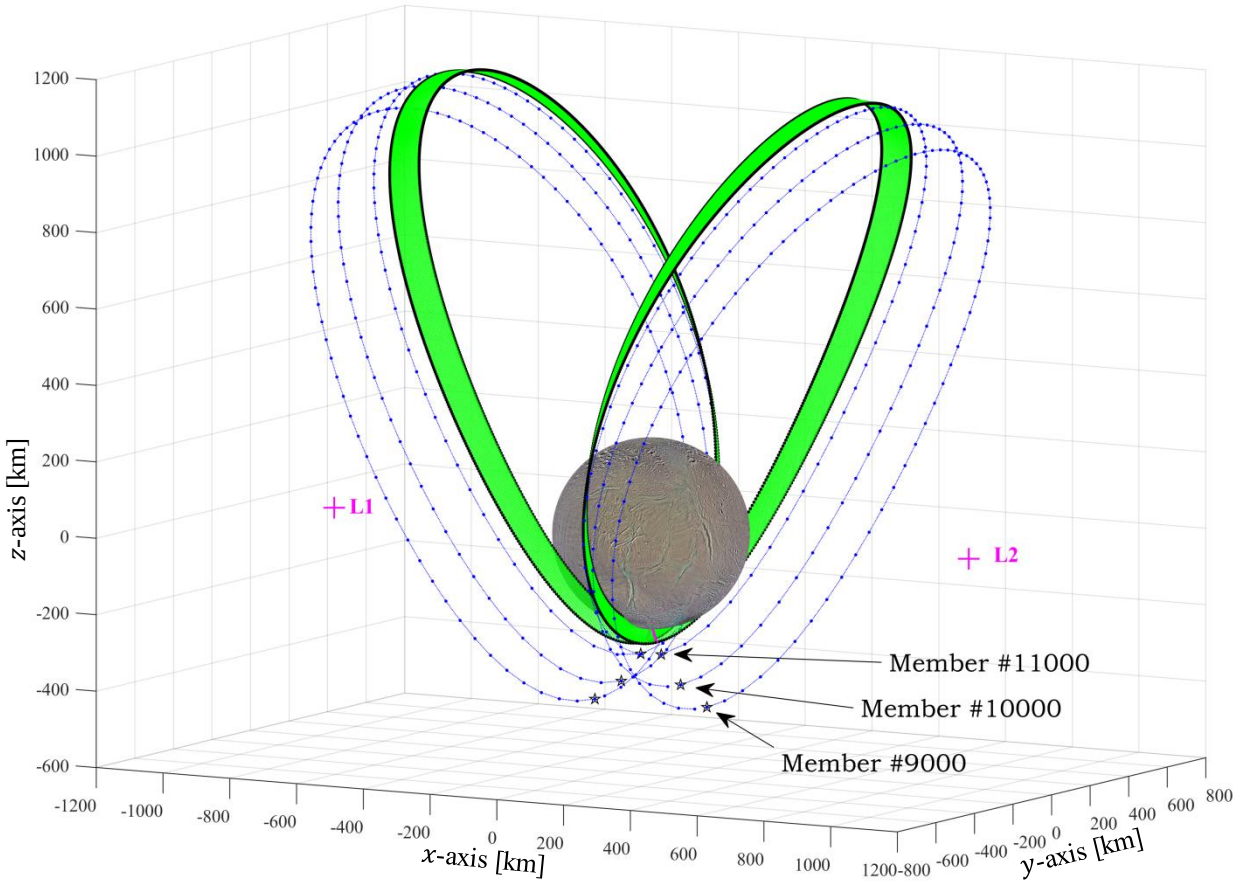

Figure 8: The graphical representation of the geometry for all periodic solutions having zeroth-order instability in the Southern Halo family at the L1/L2 points. Note that same results hold for the Northern Halo family, but those ones are not so interesting since performing fly-bys maneuvers on the northern hemisphere, where cry-volcanic activity is absent or less evident than activity in the Tiger Stripes region.

At this point we can consider the members of the Southern Halo family that have zeroth-order instability, being the member-sets {11380-11998} and {11359-11978} for L1 and L2, respectively.

V. Resonance solutions in the ER3BP

Considering here the set of solutions previously described, it is possible to investigate their orbital motion in terms of periodicity. In particular for both Halo families (at L1 and L2) we consider the minimum altitude over the Enceladus surface modeled as a sphere of 252.1 km radius. This assumption is not actually correct and the three body-axes of this icy moon are known to be different. Nonetheless, for the purpose of this analysis, we will consider such a simplified spherical model to further discuss the set of linearly stable solutions.

In Figure 9, the altitude over Enceladus is plotted against the orbital period expected for each Halo trajectory. In addition to that, some resonance periods have been highlighted, referring to the fraction with respect to the orbital revolution of Enceladus around Saturn (see Table 2). It is interesting to note that the Southern Halo periodic solution proposed by Russell and Lara [29], with a period of around 723 minutes, lies at the boundary of this set containing periodic stable solutions with zeroth-order instability.

The combinations of N and M defined in Eq. (18) are here limited since for high values of N we have a much longer orbital period for the S/C, a factor that can limit the rate of passages over the Tiger Stripes region. Moreover, also from a computational point of view, the convergence of the numerical continuation to the ER3BP depends on the integration period. For resonance solutions with N large, the period will be large and most likely will be unstable during the correction step with the modified DC-algorithm. We limit $N \leq 10$ revolutions (almost two weeks).

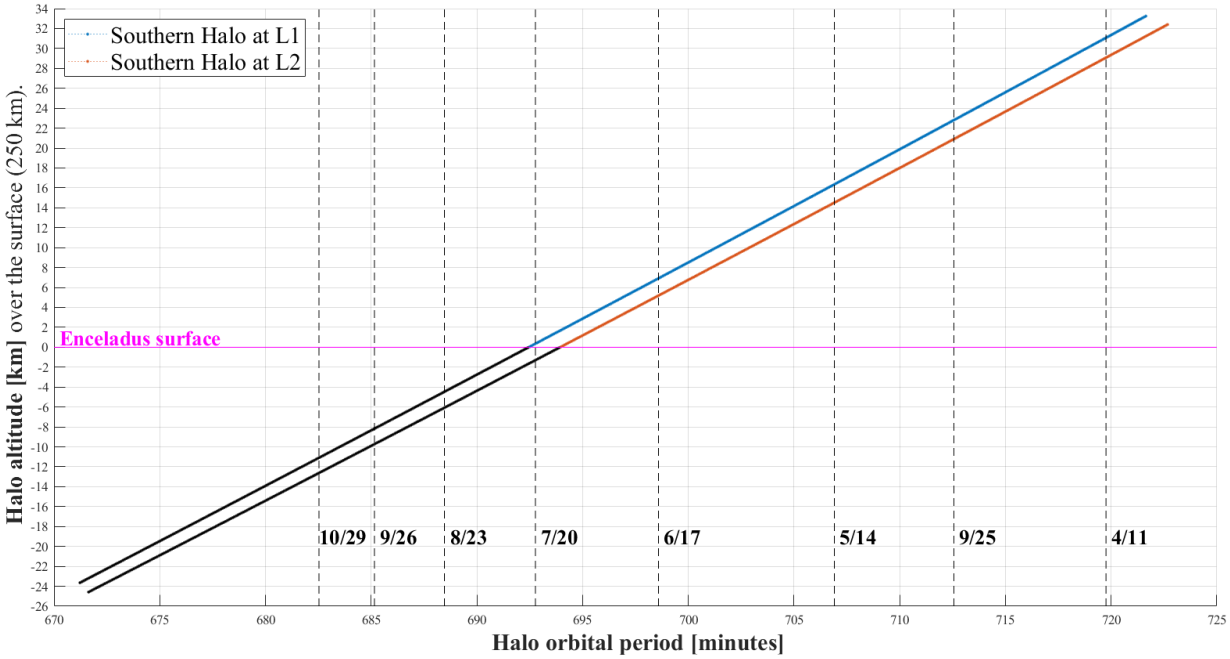

Figure 9: The altitude of linearly stable periodic solutions in the Southern Halo family is given considering Enceladus as a sphere with 252.1 km of mean radius. The minimum altitude is compared against the orbital period of each solution, and resonance candidates hitting the satellite's surface have been colored in black.

The most suitable resonance solutions for both Halo families at L1 and L2 are the ones with revolution period as {6/17, 5/14, 9/25, 4/11}. The resonance solution {7/20} is controversial due to the fact that it theoretically could hold for the Halo family at L1, thus substantially depending on the actual geometry of Enceladus. The latter has been here simplified but further investigations could allow assessing the feasibility of its use. Another aspect to be considered is that in the formulation used here, CR3BP and ER3BP models do not take into account oblateness effects. Those perturbations are fundamental and will largely affect the orbital motion, especially for closed trajectories with an altitude below 34 km.

In Table 3, the shooting conditions for these four resonance solutions are given for both L1 and L2, thus referring to non-dimensional coordinates of the CR3BP relative to this specific μ-value. Moreover, the approximate minimum altitude is shown for each solution considering only feasible trajectories that will not impact with Enceladus' surface.

Table 3: The initial conditions are given for the four resonance Halo solutions that have been identified in the zeroth-order instability region near Enceladus. The resonance parameters N and M are listed, as described in the text, along with an approximated altitude over the Enceladus mean radius (here 252.1 km).

Altitude \ Halo L1	**N**	**M**	**Shooting x_0 [-]**	**Shooting z_0 [-]**	**Shooting v_{y0} [-]**
~ 31.351 km	4	11	0.999937552716232	-0.00118728429669647	-0.0168276813565369
~ 23.076 km	9	25	0.999950255760693	-0.00115314021509136	-0.0171124618144835
~ 16.616 km	5	14	0.999959473680921	-0.00112638778947355	-0.0173426273074953
~ 7.180 km	6	17	0.999971870847787	-0.00108717260003120	-0.0176923529120416
Altitude \ Halo L2	**N**	**M**	**Shooting x_0 [-]**	**Shooting z_0 [-]**	**Shooting v_{y0} [-]**
~ 29.352 km	4	11	1.000062853735440	-0.00117884381145460	0.0168877463349484
~ 21.167 km	9	25	1.000050323704250	-0.00114508450748597	0.0171721668270576
~ 14.778 km	5	14	1.000041224007450	-0.00111863600970700	0.0174020137465557
~ 5.447 km	6	17	1.000028974373470	-0.00107987055384213	0.0177511922561054

Before the extension of a resonance solution into the ER3BP, its linear stability can be checked over the expected period T_E relatively to the Elliptic case, as given in Eq. (18). Moreover, from a stability point of view, the characteristic multipliers can be still analyzed for this solution, but they will be computed over M revolutions since this is the period needed by that solution to be valid within the ER3BP model (see Ref. [34]). Considering the largest eigenvalues (in magnitude) for the CR3BP, it follows that for the ER3BP we have

$$|\lambda_{MAX}|_{ER3BP} = (|\lambda_{MAX}|_{CR3BP})^M \tag{20}$$

and this can confirm what stated regarding the (linear) stability of solution with a very long period. Especially when considering numerical errors, an eigenvalue with a module exceeding "one" by 0.001 will approximately be M times larger in the ER3BP. This is a rule of thumb that can be proved by making use of the previous Eq. (20). For what concerns the previous solutions, it is found that the largest eigenvalue's module exceeds "one" by

- 2.5e-03 (L1) and 3.6e-03 (L2) for the N4M11 resonance orbit;
- 3.1e-11 (L1) and 5.9e-03 (L2) for the N9M25 resonance orbit;
- 3.7e-12 (L1) and 7.9e-11 (L2) for the N5M14 resonance orbit;
- 1.6e-04 (L1) and 2.0e-11 (L2) for the N6M17 resonance orbit.

B. Elliptic Halo solutions in the ER3BP

The two resonance solutions for N = 5 and M = 14 have been tested, where the periodicity holds for hundreds of revolutions, therefore being a perfect candidate for the numerical continuation into the ER3BP. Given that M is even, it follows from Table 1 that this solution bifurcates into a left-Halo and right-Halo periodic trajectory within the ER3BP. In fact, considering for the elliptic case the orbital period T_E in Eq. (18), we see that the initial condition at $e = 0$ is the same whether we starts at $\theta_0 = 0$ or $\theta_0 = \pi$. The same is not true for cases when M is odd, thus leading to the so-called apo-Halo and peri-Halo solutions. [34]

The two solutions (left/right) depends upon the initial condition starting within the xz-plane. The initial time is still set as $\theta_0 = 0$ for both cases, while the shooting point can be found in each of the two intersections of the Halo family previously generated. The symmetry with respect to the xy-plane is still valid and both Southern/Northern solutions are admitted. In our case, we focus on the Southern type for the mission constrains discussed before, and so we continue considering for each L-point two shooting conditions. The latter are then numerically continued till reaching the eccentricity mean value that has been given in Table 2.

The numerical continuation of the N5M14 resonance solution shows a very different behavior when starting at the intersection closer or farther from Enceladus (see Figure 8). In fact in the bifurcation, also the instability order changes and this can lead to a divergence of the modified DC-algorithm. Nonetheless, a solution for each Lagrange point was found, being part of the left-group since having a positive and negative shooting v_{y0} velocity for L1 and for L2, respectively. In Table 4 the conditions for the generation of the left-Halo (Southern) solution are given and compared (in non-dimensional units) to the respective shooting conditions found in the CR3BP. To observe that these results refers to a specific μ-value here adopted, as also the fact that resonance conditions changes depending on the revolution period between primary and secondary masses. This dependency makes the ER3BP no more independent from the semi-major axis value that was not considered at all in the CR3BP model.

Table 4: The shooting conditions are given in non-dimensional coordinates for the Southern Halo family with resonance N5M14 in the CR3BP. In the ER3BP the family bifurcates, and here the two left-Halo solutions (for L1 and L2) are given. Initial time for these conditions is $\theta_0 = 0$, so when Enceladus is at the perigee.

L-point	Model	Family	Shooting x_0 [-]	Shooting z_0 [-]	Shooting v_{y0} [-]
L1	CR3BP	Halo	+ 0.997477387363711	– 0.0048864999370884	+ 0.0053770757276075
L1	ER3BP	Left-Halo	+ 0.997517723018798	– 0.0047932140335318	+ 0.0055207157334874
L2	CR3BP	Halo	+ 1.002503133204690	– 0.0048942604359270	– 0.0053471516259500
L2	ER3BP	Left-Halo	+ 1.002453755567898	– 0.0047714680888800	– 0.0055303171375790

At this point, we present a brief analysis performed using an ephemeris model in order to assess the feasibility of such solutions in a more realistic scenario.

C. Validation of the solutions using an ephemeris model

The resonance solutions discussed so far have been integrated by using a precise orbit integrator. In the simulation setup we considered only Saturn and Enceladus as point masses with the standard gravitational parameters as listed in Table 2, i.e. the spacecraft has only two gravity nodes. As mentioned, the DE438 has been used for the planetary ephemerides, while the SAT425 has been used for the Saturn satellite ephemerides.

We have firstly verified that considering relativistic effects and gravitational attraction from other bodies in the Solar System has a negligible impact on the propagation of the orbit for the time-span of interest. On the other hand, the oblateness of both Saturn and Enceladus can have a significant effect on orbital stability. In particular, Saturn has a large value of J2, in the spherical harmonic gravity expansion, equal to 16290.573 ± 0.028e-6 and to 5435.2 ± 34.9 for Saturn and Enceladus, respectively [62]. Higher orders of the gravity spherical harmonic expansion are expected to be negligible. Anyhow, a careful analysis is needed in order to assess the stability considering also the oblateness perturbations.

In the realistic scenario we compare the effects of a shooting condition violating constrains on the shooting time, here being $\theta_0 = 0$ for all solutions. It follows that we should start at a point where Enceladus is at the perigee of the quasi-Keplerian motion described around Saturn. The starting time for the simulation found on the 15th of November was set at around 00:04:45 (Barycentric Dynamical Time, or TDB), while we tested the same solution for a different starting time. In particular, we considered an initial time for Enceladus at its apogee during the same day (at around 16:32:59 TDB) in order to highlight possible effects on the solution for the ER3BP.

The results are given for the left-Halo solution at L1, with similar results as for the solution at L2. As it can be noted, the adoption of an ephemeris model destroys pretty quickly the periodicity, while surely the same exact initial condition behaves much differently when constrains on the shooting time is not fulfilled. This can be physically explained by the fact that the shooting velocity in Table 4 refers to a rotating frame and the angular velocity in the ER3BP can change substantially when the eccentricity is large enough. This is directly visible in the Eq. (2), while in the Figure 10 the S/C radial distance from Enceladus is represented for visualizing this added instability.

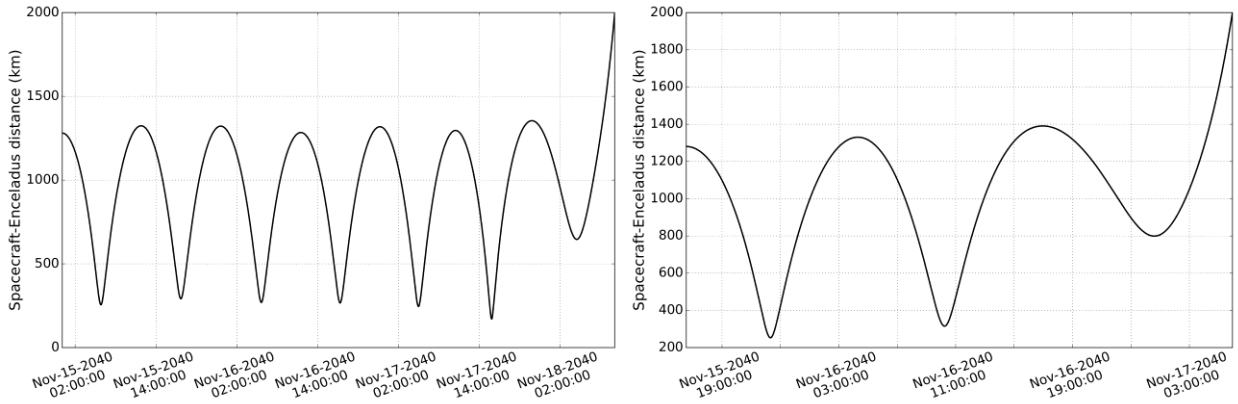

Figure 10: Results of simulations in a realistic scenario using the ephemerides model, where we compare the same initial condition for the left-Halo solution at L1 for two shooting times respectively as $\theta_0 = 0$ (LEFT) and $\theta_0 = \pi$ (RIGHT). The radial distance from Enceladus, and its periodicity, is represented over time.

VI. Conclusions

In this research work we have analyzed linearly stable orbits around the Saturn's moon Enceladus. The interest about the exploration of this moon has increased after the discovery of the plume ejecta by the Cassini mission. Several mission scenarios have been investigated in the past, and many more concepts are most likely going to be proposed in the next few years, following the recent discoveries at the so-called Tiger Stripes region. The mission design is not trivial, while complicated by the unstable dynamics near Enceladus. In fact, the vicinity of Saturn, being much heavier, causes large perturbations to the S/C motion. The latter was studied by considering solutions orbiting around Enceladus, mostly in resonance with its orbital motion around Saturn.

The analysis presented here started with an analysis of the Saturn-Enceladus system based a CR3BP model, which assumes that the two celestial bodies orbit around their mutual barycenter in circular trajectories. Several families of solutions can be found near the equilibrium points of the system, especially looking at the L1/L2 points that are less than 1000 km away from Enceladus. The continuity of these families is guaranteed by the symplectic nature of the problem, therefore having an infinite set of possible trajectory for the mission orbit design. The latter has been considered in support to low-altitude fly-by operations in order to sample material ejected at the Tiger Stripes region, near the Enceladus South Pole.

The spectral stability has been studied, showing that only suitable solutions are all part of the Halo family, more precisely the Southern Halo one. The latter exist at both L1 and L2 points, while having similar characteristics and treated in the past researches by using a Hill model. We considered an analysis on members of this family generated near the Lagrange points and numerically continued till reaching Enceladus surface.

The linearly stable region has also favorable geometric characteristics since very close to the surface of Enceladus, here assumed as a sphere-shaped body. Nonetheless, within this set of periodic solutions, some of the trajectories have been identified as in resonance with Enceladus motion around Saturn. This fact is relevant due to the fact that in the elliptic problem those resonance solutions hold, while the continuity of each periodic family is destroyed. Some of these resonance solutions are discarded since impacting with Enceladus surface, while four different resonance orbits were identified.

Considering one of the previous solution, here being defined a N5M14 (N as Enceladus revolutions, M as S/C revolutions), the analysis of its linear stability showed favorable characteristics for being extended to the ER3BP model. The latter is again based on a numerical continuation in the eccentricity parameter, while a bifurcation of the solutions has been also discussed. The selected orbits can be found as a Left-Halo or Right-Halo solution, the former being more stable and so further discussed in this work.

The solution is then analyzed with a precise orbit integrator making use of latest planetary and satellite ephemeris. In this way, it can be noted that the conditions defined by the ER3BP are really important for achieving more reliable periodic solutions. Moreover, differently from an ideal ER3BP model, the large time-variations of the eccentricity (due to resonance effects with another Saturn's satellite, here Dione) lead to unstable orbits. This time-variation should be taken into account and investigated in future researches by developing an ER3BP model that takes into accounts these non-negligible effects.

Acknowledgments

This research was initiated during the 2019 Caltech Space Challenge. The authors would like to thank the 2019 Caltech Space Challenge organizers Fabien Royer and Simon Toedtl together with all the participants and the mentors for the meaningful discussions.

References

[1] Satellites of Saturn, Monthly Notices of the Royal Astronomical Society, Volume 8, Issue 3, January 1848, Pages 42–43, https://doi.org/10.1093/mnras/8.3.42

[2] Spencer, J. R., Pearl, J. C., Segura, M., Flasar, F. M., Mamoutkine, A., Romani, P., ... & Lopes, R. M. C. (2006). Cassini encounters Enceladus: Background and the discovery of a south polar hot spot. Science, 311(5766), 1401-1405.

[3] Cortright, E. M. (1967). The Voyager program. NASA Technical Reports Server ID19670046503

[4] Stone, E. C., & Miner, E. D. (1981). Voyager 1 encounter with the Saturnian system. Science, 212(4491), 159-163.

[5] Stone, E. C.; Miner, E. D. (29 January 1982). "Voyager 2 Encounter with the Saturnian System" (PDF). Science. 215 (4532): 499–504. Bibcode:1982Sci...215..499S. doi:10.1126/science.215.4532.499. PMID 17771272

[6] Matson, D. L., Spilker, L. J., & Lebreton, J. P. (2003). The Cassini/Huygens mission to the Saturnian system. In The Cassini-Huygens Mission (pp. 1-58). Springer, Dordrecht.

[7] Kerr, R. A. (2005). Cassini catches mysterious hot spot on icy-cold Enceladus. Science, 309(5736), 859-860.
[8] Dougherty, M. K., Khurana, K. K., Neubauer, F. M., Russell, C. T., Saur, J., Leisner, J. S., & Burton, M. E. (2006). Identification of a dynamic atmosphere at Enceladus with the Cassini magnetometer. Science, 311(5766), 1406-1409.
[9] Hansen, C. J., Esposito, L., Stewart, A. I. F., Colwell, J., Hendrix, A., Pryor, W., ... & West, R. (2006). Enceladus' water vapor plume. Science, 311(5766), 1422-1425.
[10] Porco, C. C., Helfenstein, P., Thomas, P. C., Ingersoll, A. P., Wisdom, J., West, R., ... & Kieffer, S. (2006). Cassini observes the active south pole of Enceladus. Science, 311(5766), 1393-1401.
[11] Jennings, D. E., Flasar, F. M., Kunde, V. G., Nixon, C. A., Segura, M. E., Romani, P. N., ... & Mamoutkine, A. A. (2017). Composite infrared spectrometer (CIRS) on Cassini. Applied Optics, 56(18), 5274-5294.
[12] Waite, J. H., Combi, M. R., Ip, W. H., Cravens, T. E., McNutt, R. L., Kasprzak, W., ... & Magee, B. (2006). Cassini ion and neutral mass spectrometer: Enceladus plume composition and structure. Science, 311(5766), 1419-1422.
[13] Waite Jr, J. H., Teolis, B. D., Perry, M. E., Bouquet, A., Glein, C., & Perryman, R. (2015, December). Enceladus Flyby 21: The Final Cassini INMS Flyby. In AGU Fall Meeting Abstracts.
[14] National Academies of Sciences, Engineering, and Medicine. 2018. Visions into Voyages for Planetary Science in the Decade 2013-2022: A Midterm Review. Washington, DC: The National Academies Press. https://doi.org/10.17226/25186
[15] Lunine, J., Waite, H., Postberg, F., Spilker, L., & Clark, K. (2015, April). Enceladus life finder: the search for life in a habitable moon. In EGU General Assembly Conference Abstracts (Vol. 17).
[16] Eigenbrode, J., Gold, R. E., McKay, C. P., Hurford, T., & Davila, A. (2018, July). Searching for Life in an Ocean World: The Enceladus Life Signatures and Habitability (ELSAH) mission concept. In 42nd COSPAR Scientific Assembly (Vol. 42).
[17] Lorenz, R. D., Turtle, E. P., Barnes, J. W., Trainer, M. G., Adams, D. S., Hibbard, K. E., ... & Ravine, M. A. (2018). Dragonfly: a Rotorcraft Lander Concept for scientific exploration at Titan. Johns Hopkins APL Technical Digest, 34.
[18] Turtle, E. P., Barnes, J. W., Trainer, M. G., Lorenz, R. D., MacKenzie, S. M., Hibbard, K. E., ... & Zacny, K. (2017, March). Dragonfly: Exploring Titan's prebiotic organic chemistry and habitability, 48th Lunar and Planetary Science Conference, LPI Contribution No. 1964, id.1958, The Woodlands, Texas.
[19] National Research Council. 2011. Vision and Voyages for Planetary Science in the Decade 2013-2022. Washington, DC: The National Academies Press. https://doi.org/10.17226/13117
[20] Taubner, R. S., Baumann, L. M., Bauersachs, T., Clifford, E. L., Mähnert, B., Reischl, B., ... & Birgel, D. (2019). Membrane Lipid Composition and Amino Acid Excretion Patterns of Methanothermococcus okinawensis Grown in the Presence of Inhibitors Detected in the Enceladian Plume. Life, 9(4), 85.
[21] Gehrels, T., & Esposito, L. (1981). Pioneer fly-by of Saturn and its rings. Advances in Space Research, 1(8), 67-71.
[22] Casani, J. (2019). Space Fission Power: NASA's best bet to continue to explore the outer solar system, Nuclear and Emerging Technologies for Space 2019, in Richland, WA.
[23] Palma, D. F. F. (2016). "Preliminary Trajectory Design of a Mission to Enceladus". M.Sc. thesis, Instituto Superior Técnico Lisbon, Portugal.
[24] National Aeronautics and Space Administration, Mission Concept Study: Planetary Science Decadal Survey – JPL Rapid Mission Architecture (RMA) Enceladus Study Final Report, Science Champion: John Spencer, NASA HQ POC: Curt Niebur, April 2010.
[25] Kinsey, R., "Mission Concept Study: Planetary Science Decadal Survey (Enceladus Orbiter)," 2010.
[26] Strange, N., Campagnola, S., & Russell, R. (2009, December). A New Tour Design Technique to Enable an Enceladus Orbiter. In AGU Fall Meeting Abstracts.
[27] Scheeres, D. J., Guman, M. D., & Villac, B. F. (2001). Stability analysis of planetary satellite orbiters: application to the Europa orbiter. Journal of Guidance, Control, and Dynamics, 24(4), 778-787.
[28] Szebehely, V. (1967). Theory of orbits: the restricted problem of three bodies. Yale university, New Haven, CT.
[29] Russell, R. P., & Lara, M. (2009). On the design of an Enceladus science orbit. Acta Astronautica, 65(1-2), 27-39.
[30] Boone, D. R., "Integration of Geodesy Mission Design and Navigation for Planetary Satellite Orbiters" (2013). Aerospace Engineering Sciences Graduate Theses & Dissertations. 66. https://scholar.colorado.edu/asen_gradetds/66
[31] Ross, S. D., & Lo, M. W. (1998). Low Energy Interplanetary Transfers Using the Invariant Manifolds of L1, L2, and Halo Orbits. NASA Technical Report Server ID20060035581
[32] Broucke, R. (1969). Stability of periodic orbits in the elliptic, restricted three-body problem. AIAA journal, 7(6), 1003-1009.
[33] Moyer, T. D. (1971), Mathematical formulation of the Double-Precision Orbit Determination Program (DPODP), NASA Technical Report 32-1527
[34] Massarweh, L. (2016). "Linear stability and bifurcations of periodic Lagrange orbits in the Elliptic Restricted 3-Body Problem: an investigation at L1/L2 in the Earth-Moon system". M.Sc. thesis, Delft University of Technology, Netherlands.
[35] Goldstein, H., Poole, C., & Safko, J. (2002). Classical Mechanics. Person.
[36] Vallado, D. A. (2001). Fundamentals of astrodynamics and applications (Vol. 12). Springer Science & Business Media.
[37] Perko, L. (2013). Differential equations and dynamical systems (Vol. 7). Springer Science & Business Media.
[38] Verhulst, F. (2006). Nonlinear differential equations and dynamical systems. Springer Science & Business Media.
[39] Musielak, Z. E., & Quarles, B. (2014). The three-body problem. Reports on Progress in Physics, 77(6), 065901.
[40] Gómez, G., Koon, W. S., Lo, M. W., Marsden, J. E., Masdemont, J., & Ross, S. D. (2004). Connecting orbits and invariant manifolds in the spatial restricted three-body problem. Nonlinearity, 17(5), 1571.

[41] Miele, A. (1961). Theorem of image trajectories in the Earth-Moon space. In XIth International Astronautical Congress Stockholm 1960/XI. Internationaler Astronautischer Kongress/XIe Congrès International D'Astronautique (pp. 385-391). Springer, Vienna.
[42] Wintner, A. (1941). The analytical foundations of celestial mechanics. Princeton, NJ, Princeton university press; London, H. Milford, Oxford university press, 1941.
[43] Euler, L. (1767). De motu rectilineo trium corporum se mutuo attrahentium. Novi commentarii academiae scientiarum Petropolitanae, 144-151.
[44] Miele, A. (2010). Revisit of the theorem of image trajectories in the earth-moon space. Journal of optimization theory and applications, 147(3), 483-490.
[45] Howell, K. C. (1984). Three-dimensional, periodic,'halo'orbits. Celestial mechanics, 32(1), 53-71.
[46] Howell, K. C., & Pernicka, H. J. (1987). Numerical determination of Lissajous trajectories in the restricted three-body problem. Celestial Mechanics, 41(1-4), 107-124.
[47] Kolemen, E., Kasdin, N. J., & Gurfil, P. (2007, February). Quasi-Periodic Orbits of the Restricted Three-Body Problem Made Easy. In AIP Conference Proceedings (Vol. 886, No. 1, pp. 68-77). AIP.
[48] Jorba, A., & Masdemont, J. (1999). Dynamics in the center manifold of the collinear points of the restricted three body problem. Physica D: Nonlinear Phenomena, 132(1-2), 189-213.
[49] Nayfeh, A. (1973). Perturbation Methods. New York: Wiley.
[50] Richardson, D. L. (1980). Analytic construction of periodic orbits about the collinear points. Celestial mechanics, 22(3), 241-253.
[51] Breakwell, J. V., & Brown, J. V. (1979). The 'halo'family of 3-dimensional periodic orbits in the Earth-Moon restricted 3-body problem. Celestial mechanics, 20(4), 389-404.
[52] Bosanac, N. (2012). Exploring the influence of a three-body interaction added to the gravitational potential function in the circular restricted three-body problem: a numerical frequency analysis (Doctoral dissertation, Purdue University).
[53] Doedel, E. J., Romanov, V. A., Paffenroth, R. C., Keller, H. B., Dichmann, D. J., Galán-Vioque, J., & Vanderbauwhede, A. (2007). Elemental periodic orbits associated with the libration points in the circular restricted 3-body problem. International Journal of Bifurcation and Chaos, 17(08), 2625-2677.
[54] Deprit, A. (1965, July). Routh's critical mass ratio at the triangular libration centers. In Thermophysics Specialist Conference (p. 681).
[55] Feng, J., Noomen, R., Visser, P. N., & Yuan, J. (2015). Modeling and analysis of periodic orbits around a contact binary asteroid. Astrophysics and Space Science, 357(2), 124.
[56] Campagnola, S., Lo, M., & Newton, P. (2008). Subregions of motion and elliptic halo orbits in the elliptic restricted three-body problem. Proceedings of the AAS/AIAA Space Flight Mechanics Meeting held January 27, 2008, Galveston, Texas.
[57] Moulton, F.: 1920, Periodic Orbits, Carnegie Institute Publication No. 161.
[58] Acton, C.H.; "Ancillary Data Services of NASA's Navigation and Ancillary Information Facility;" Planetary and Space Science, Vol. 44, No. 1, pp. 65-70, 1996.
[59] Folkner, W. M., Williams, J. G., Boggs, D. H., Park, R. S., & Kuchynka, P. (2014). The planetary and lunar ephemerides DE430 and DE431. Interplanetary Network Progress Report, 196, 1-81.
[60] Ingersoll, A. P., Ewald, S. P., & Trumbo, S. K. (2019). Time variability of the Enceladus plumes: Orbital periods, decadal periods, and aperiodic change. Icarus.
[61] Zhang, K., & Nimmo, F. (2009). Recent orbital evolution and the internal structures of Enceladus and Dione. Icarus, 204(2), 597-609.
[62] L. Iess, D. J. Stevenson, M. Parisi, D. Hemingway, R. A. Jacobson, J. I. Lunine, F. Nimmo, J. W. Armstrong, S. W. Asmar, M. Ducci, P. Tortora (2014), The Gravity Field and Interior Structure of Enceladus, Science, Vol. 344, Issue 6179, pp. 78-80, DOI: 10.1126/science.1250551